J|A|C|S
ARTICLES

Published on Web 10/23/2009

Molecular Insights into the Self-Aggregation of Aromatic Molecules in the Synthesis of Nanoporous Aluminophosphates: A Multilevel Approach

Luis Gómez-Hortigüela,*[,†,‡] Said Hamad,[§] Fernando López-Arbeloa,[||] Ana B. Pinar,[‡] Joaquín Pérez-Pariente,[‡] and Furio Corà[†]

Department of Chemistry, Third Floor, Kathleen Lonsdale Building, University College London, Gower Street, WC1E 6BT, London, United Kingdom, Instituto de Catálisis y Petroleoquímica-CSIC, C/ Marie Curie 2, 28049 Cantoblanco, Madrid, Spain, Department of Physical, Chemical and Natural Systems, University Pablo de Olavide, Utrera Road Km 1, 41013 Seville, Spain, and Departamento de Química Física, Universidad del País Vasco-EHU, Apartado 644, 48080 Bilbao, Spain

Received July 22, 2009; E-mail: lhortiguela@icp.csic.es

Abstract: Fluorescence spectroscopy and a range of computer simulation techniques are used to study the structure directing effect of benzylpyrrolidine (BP) and (*S*)-(−)-*N*-benzylpyrrolidine-2-methanol (BPM) in the synthesis of nanoporous aluminophosphate frameworks with AFI (one-dimensional channels) and SAO (three-dimensional interconnected channels) topologies. We study the supramolecular chemistry of BP and BPM molecules in aqueous solution and compare it with the aggregation state of the molecules found when they are inside the AlPO nanopores after crystallization. The aggregation of the molecules within the structures can be explained by a combination of thermodynamic and kinetic effects. The former are given by the stability of the molecular species interacting with the oxide networks relative to their stability in solution; the latter depend on the aggregation behavior of the molecules in the synthesis gels prior to crystallization. Whereas BPM only forms one type of aggregate in solution, which has the appropriate conformation to match the empty channels of the forming nanoporous frameworks, BP forms aggregates with different molecular orientations, of which only one matches the framework interstices. This different supramolecular chemistry, together with the higher interaction of BPM with the oxide networks, makes BPM a better structure directing agent (SDA); it is also responsible for the higher incorporation of BPM as dimers in the frameworks, especially in the AFI structure, observed experimentally. The concentration of the SDA molecules in the gels, and so the density per volume of the SDAs, determines the exclusion zone from which the pores and/or cavities of the framework will arise, and so the porous network of the formed material. A clear relationship between the SDA density in solution and in the framework is observed, thus enabling an eventual control of the material density by adjusting the SDA concentration in the gels. The topological instability intrinsic to these open framework structures is compensated by a high host−guest interaction energy; the SAO topology is further stabilized by doping with Zn. Our computational results account for and rationalize all the effects observed experimentally, providing a complete picture of the mode of structure direction of these aromatic molecules in the synthesis of nanoporous aluminophosphates.

Introduction

Nanoporous materials have been widely employed industrially in molecular sieving, ion-exchange, and catalytic applications,[1−3] which exploit the molecular dimensions and the crystalline nature of the nanoporous structure to discriminate between molecules with very subtle steric differences. Since the discovery of nanoporous aluminophosphates ($AlPO_4$) by Wilson et al. in 1982,[4] the synthesis of these materials has been widely studied, yielding a diversity of structural types comparable to that of the previously known aluminosilicate-based zeolites.[5] In these $AlPO_4$ materials, there is a strict alternation of Al^{3+} and P^{5+} ions. In contrast to hydrophobic SiO_2 zeolites, AlPO frameworks are more hydrophilic due to the molecular-ionic nature of the network, which can be seen as Al^{3+} and PO_4^{3-} ions ionically bonded.[6] Both Al and P ions can be isomorphically replaced by heteroatoms, giving rise to acid, redox and even bifunctional properties to the nanoporous materials, which provide a wide range of potential applications.

† University College London.
‡ Instituto de Catálisis y Petroleoquímica-CSIC.
§ University Pablo de Olavide.
|| Universidad del País Vasco-EHU.

(1) Davis, M. E. *Acc. Chem. Res.* **1993**, *26*, 111.
(2) Naber, J. E.; de Jong, K. P.; Stork, W. H. J.; Kuipers, H. P. C. E.; Post, M. F. M. *Stud. Surf. Sci. Catal.* **1994**, *84C*, 2197.
(3) Venuto, P. B. *Microporous Mesoporous Mater.* **1994**, *2*, 297.
(4) Wilson, S. T.; Lok, B. M.; Flanigen, E. M. US Patent, 4310440, 1982.
(5) Baerlocher, Ch.; McCusker, L. B. Database of Zeolite Structures. http://www.iza-structure.org/databases/ (accessed October 20, 2009).
(6) Corà, F.; Alfredsson, M.; Barker, C. M.; Bell, R. G.; Foster, M. D.; Saadoune, I.; Simperler, A.; Catlow, C. R. A. *J. Solid State Chem.* **2003**, *176*, 496.

The synthesis of nanoporous materials is based on hydrothermal methods, where the source of the inorganic ions, water (or eventually other solvents) and, generally, an organic molecule are heated for a certain time. The inclusion of the organic molecules is usually required to direct the crystallization of a certain nanoporous structure, and so they are called structure directing agents (SDAs). The role of these organic molecules has been traditionally described as a "template effect"[7] to indicate that the organic molecules organize the inorganic tetrahedral units into a particular topology around themselves during the nucleation process, providing the initial building blocks from which crystallization of the nanoporous structures will take place. Nevertheless, new theories[8−11] based on experimental evidence[12,13] are currently emerging suggesting that the role that SDA molecules play during crystallization of nanoporous materials is more complex than the one described in the initial template theory. The exact role of the SDAs is still far from being properly understood, and structure direction is a major open issue in molecular sieves science. Controlling this feature would enable the synthesis of new topologies, as well as to gain control over crystal sizes and morphologies and the location of heteroatoms, if present.

The organic SDA molecules are encapsulated within the nascent nanoporous structure as it crystallizes, developing strong nonbonded interactions with the framework and thus contributing to the final stability of the system. It is well-known that nanoporous frameworks are metastable systems, and their intrisic stability increases with the framework density, that is, denser materials are more stable than open-frameworks. The organic molecules occluded within the void spaces of open-frameworks interact with the surrounding oxide network providing the required thermodynamic stabilization to make viable the crystallization of such structures. Therefore, the SDA molecules direct the crystallization of the nanoporous frameworks not only by providing a volume from which the inorganic ions are excluded, but also by altering the relative thermodynamic stability of different framework structures via the development of different SDA-framework interactions.

To be efficient SDAs, organic molecules are required to be moderately hydrophobic,[14] be soluble in the synthesis media (but not interact strongly with the solvent), be moderately rigid (to increase selectivity in structure direction), have high hydrothermal stability and develop strong nonbonded interactions with the nanoporous structure within which they will be occluded. In a search for new large-pore nanoporous structures, interesting for applications involving large molecules, increasingly larger and more complex SDAs have been used, leading to the discovery of a number of new zeolitic topologies.[15] However, despite the large number of SDAs of very different sizes and shapes used up to date, their choice as SDAs has almost invariably considered the features of single molecular units. Supramolecular chemistry has only rarely been mentioned in the structure direction environment,[16] in contrast to the wide use of, for example, supramolecular micellar arrangements in the synthesis of mesoporous materials.[17] In this context, a new concept in structure direction of nanoporous materials has been recently proposed by us[18−21] and by Corma et al.,[22] consisting in the use of supramolecular self-assembled molecular aggregates as SDA. This new concept of structure direction can be achieved in practice using aromatic molecules, that self-assemble with their aromatic rings parallel to each other through $\pi-\pi$ type interactions, these supramolecular entities being the actual structure directing agent of the nanoporous structure. This mode of structure direction permits the use of relatively simple molecules with suitable size, rigidity, thermal stability and hydrophobicity properties to create larger void structures and more complex zeolitic topologies due to their supramolecular aggregation.

Examples of molecules susceptible of self-assembling that we have recently been studying are benzylpyrrolidine (BP) and the related (*S*)-(−)-*N*-benzylpyrrolidine-2-methanol (BPM) (Figure 1, bottom). Recent work carried out in our laboratories demonstrated that these molecules are able to direct the crystallization of the AFI and SAO large-pore frameworks depending on the SDA concentration in the synthesis gels:[23−25] an SDA concentration in the gel of 1 SDA:40 H_2O leads to the crystallization of the AFI structure, while increasing the SDA concentration to 2 SDA:40 H_2O leads to the crystallization of the SAO structure, for both BP and BPM SDAs. Moreover, a combination of fluorescence spectroscopy and computational simulations allowed us to gain insights into the supramolecular chemistry involved in the occlusion of BP and BPM as monomeric or dimeric species within the AFI structure: we observed that BPM is incorporated preferentially as dimers, whereas BP tends to be occluded mostly as monomers, although dimers are required for the nucleation step to occur.[20] In the present work, using again a combination of fluorescence spectroscopy and atomic-level modeling, we study the aggregation behavior of the two molecules in the synthesis gels, which are simulated as concentrated solutions of the SDA molecules at the same molar composition as in the gels, and within the nanoporous frameworks. Our goal is to relate the supramolecular chemistry observed in the solutions with the mode of occlusion of the SDA molecules as monomeric or dimeric species within the AFI and SAO structures. We also employ a recently developed computational model for predicting the stabilization provided by the simultaneous occlusion of water molecules in

(7) Gies, H.; Marler, B. *Zeolites* **1992**, *12*, 42.
(8) Caratzoulas, S.; Vlachos, D.; Tsapatsis, M. *J. Phys. Chem. B* **2005**, *109*, 10429.
(9) Caratzoulas, S.; Vlachos, D.; Tsapatsis, M. *J. Am. Chem. Soc.* **2006**, *128*, 596.
(10) Caratzoulas, S.; Vlachos, D.; Tsapatsis, M. *J. Am. Chem. Soc.* **2006**, *128*, 16138.
(11) Caratzoulas, S.; Vlachos, D. *J. Phys. Chem. B* **2008**, *112*, 7.
(12) Kinrade, S. D.; Knight, C. T. G.; Ple, D. L.; Syvitski, R. *Inorg. Chem.* **1998**, *27*, 4272.
(13) Kinrade, S. D.; Knight, C. T. G.; Ple, D. L.; Syvitski, R. *Inorg. Chem.* **1998**, *27*, 4278.
(14) Kubota, Y.; Helmkamp, M. M.; Zones, S. I.; Davis, M. E. *Microporous Mater.* **1996**, *6*, 213.
(15) Zones, S. I.; Hwang, S.-J.; Elomari, S.; Ogino, I.; Davis, M. E.; Burton, A. W. *C.R. Chimie* **2005**, *8*, 267.
(16) Xu, R.; Zhang, W.; Guan, J.; Yunpeng, X.; Wang, L.; Ma, H.; Zhijian, T.; Han, X.; Lin, L.; Bao, X. *Chem.—Eur. J.* **2009**, *15*, 5348.
(17) Cheng, C.-G.; Luan, Z.; Klinowski, J. *Langmuir* **1995**, *11*, 2815.
(18) Gómez-Hortigüela, L.; Corà, F.; Catlow, C. R. A.; Pérez-Pariente, J. *J. Am. Chem. Soc.* **2004**, *126*, 12097.
(19) Gómez-Hortigüela, L.; Corà, F.; Catlow, C. R. A.; Pérez-Pariente, J. *Phys. Chem. Chem. Phys.* **2006**, *8*, 486.
(20) Gómez-Hortigüela, L.; López-Arbeloa, F.; Corà, F.; Pérez-Pariente, J. *J. Am. Chem. Soc.* **2008**, *130*, 13274.
(21) Gómez-Hortigüela, L.; Pérez-Pariente, J.; López-Arbeloa, F. *Microporous Mesoporous Mater.* **2009**, *119*, 299.
(22) Corma, A.; Rey, F.; Rius, J.; Sabater, M. J.; Valencia, S. *Nature* **2004**, *431*, 287.
(23) Gómez-Hortigüela, L.; Pérez-Pariente, J.; Blasco, T. *Microporous Mesoporous Mater.* **2005**, *78*, 189.
(24) Gómez-Hortigüela, L.; Pérez-Pariente, J.; Blasco, T. *Microporous Mesoporous Mater.* **2007**, *100*, 55.
(25) Pinar, A. B.; Gómez-Hortigüela, L.; Pérez-Pariente, J. Manuscript in preparation.

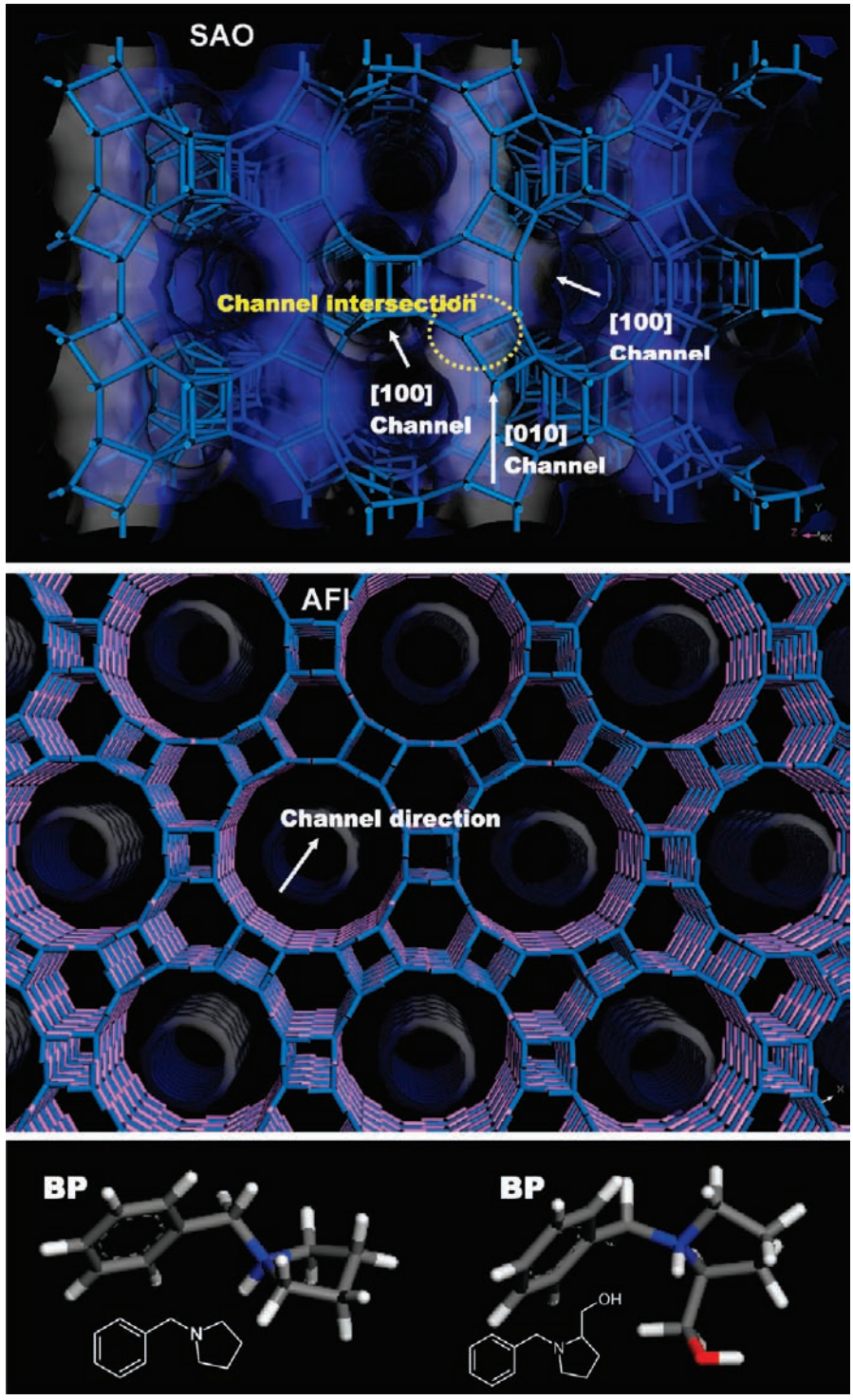

Figure 1. SAO (top) and AFI (middle) framework structures, showing the pore systems (blue-white surfaces). The oxygen atoms have been removed for the sake of clarity. (Bottom) Molecular structure of benzylpyrrolidinium (BP, left) and (*S*)-(−)-*N*-benzylpyrrolidinium-2-methanol (BPM, right).

the two frameworks[26,27] to determine the most stable arrangements of the guest (SDA and water) species within the structures and examine the effect of doping the AFI and SAO structures with Zn. The energetic balance that makes viable the crystallization of the two metastable AFI and SAO structures is examined in detail.

To better understand the inclusion of the organic and water molecules in the nanoporous architectures, we briefly describe here the porous networks of the SAO and AFI structures, shown in Figure 1. The AFI type structure is composed of one-dimensional not-interconnected 12 membered ring (MR) channels with a diameter of 7.3 Å, which are surrounded by smaller one-dimensional 4 and 6 MR channels; its framework density is 16.9 T/1000 Å^3 (T refers to framework tetrahedral Al and P

(26) Gómez-Hortigüela, L.; Pérez-Pariente, J.; Corà, F. *Chem.—Eur. J.* **2009**, *15*, 1478.
(27) Gómez-Hortigüela, L.; Pinar, A. B.; Pérez-Pariente, J.; Corà, F. *Chem. Mater.* **2009**, *21*, 3447.

sites). SDA molecules can only be hosted in the large 12 MR channels, while water molecules are small enough to be accommodated in the 12 or in the side 6 MR channels; 4 MR channels are too small to accommodate any of the guest species. Instead, the SAO structure is composed by a three-dimensional channel system, with two interconnecting 12 MR channel systems running perpendicular to each other, one along the [100] direction with a dimension of 6.5 × 7.2 Å and the other along the [001] direction with a dimension of 7.0 × 7.0 Å, giving a framework density of 13.4 T/1000 $Å^3$, one of the lowest values among known AlPO structures. SDA and water molecules can be accommodated in both channels systems and/or in the channel intersections.

Experimental Details

Details of the synthesis and characterization of benzylpyrrolidine (BP) have been given elsewhere;[23] (*S*)-(−)-*N*-benzylpyrrolidine-2-methanol (BPM) was purchased from Sigma-Aldrich. Aqueous solutions of BP and BPM molecules were prepared by adding equimolar amounts of the corresponding organic amine and HCl. In this way, 0.1, 1, and 2 M aqueous solutions of benzylpyrrolidinium chloride and (*S*)-(−)-*N*-benzylpyrrolidinium-2-methanol chloride were obtained and studied by fluorescence spectroscopy; the SDA concentrations of 1 and 2 M correspond approximately to those in the synthesis gels for AFI (1 SDA:40 H_2O) and SAO (2 SDA:40 H_2O), respectively.

The syntheses of the AFI structure by using BP and BPM as SDAs have also been reported in previous works;[23,24] details of the synthesis of the SAO structure with these molecules will be published elsewhere.[25] The SAO materials have been synthesized as Zn-doped aluminophosphates; to reduce the number of variables, Zn-doped AFI frameworks were also studied. For the Zn-doped AFI structure obtained with BPM, the molar composition was of 1 BPM:0.22 ZnO:0.89 Al_2O_3:1 P_2O_5:40 H_2O. However, BP did not lead to the crystallization of pure ZnAPO-5; therefore, in this case an undoped AlPO-5 material was studied, which was prepared with a molar composition of 1 BP:1 Al_2O_3:1 P_2O_5:40 H_2O (note that the SDA concentration is the same in both cases). In contrast, a higher concentration of SDAs was required for the synthesis of Zn-doped SAO; in this case, synthesis gels were prepared with a molar composition of 2 SDA:0.36 ZnO:0.82 Al_2O_3:1 P_2O_5:40 H_2O. The gels were introduced into 60 mL Teflon lined stainless steel autoclaves and heated statically at 423 K for 24 h. The resulting solids were separated by filtration, washed with ethanol and water, and dried at 333 K overnight.

The crystallization of the AFI and SAO structures was assessed by X-ray diffraction (Seifert XRD 3000P diffractometer, Cu Kα radiation). The organic content of the samples was studied by chemical CHN analysis (Perkin-Elmer 2400 CHN analyzer) and thermogravimetric analysis (TGA) (Perkin-Elmer TGA7 instrument).

The aggregation state of the molecules in solution and in the solid samples was studied by fluorescence spectroscopy. Liquid and solid state UV−visible fluorescence excitation and emission spectra were recorded in a SPEX fluorimeter model Fluorolog 3−22 equipped with a double monochromator in both the excitation and the emission channels and a red-sensitive photomultiplier detector operating with a Peltier-cooling system. The fluorescence spectra were registered in the front-face configuration in which the emission signal was detected at 22.5° with respect to the excitation beam. Liquid solutions were placed in 1-mm pathway quartz cells whereas the fluorescecence spectra of the solid aluminophosphate samples were recorded by means of thin films supported on glass slides by solvent evaporation from a dichloromethane suspension.

Computational Details. The aggregation behavior of the SDA molecules both in aqueous solution and within the nanoporous frameworks was studied computationally to understand the molecular features governing the supramolecular chemistry that drives the incorporation of these molecules within the nanoporous solids as monomers or dimers. Molecular structures of the SDAs and water molecules, and their interaction with the nanoporous aluminophosphate frameworks, were described with the cvff forcefield,[28] which has been successfully applied recently for the simulation of zeolite host−guest systems[29−31] and water containing systems.[32] The AFI and SAO framework atoms were kept fixed during all the calculations involving guest molecules. Due to the very acidic pH (typical pH ≈ 3−4), SDA molecules are expected to be protonated in the synthesis gels (the pK_a of BP in water at 25 °C is 9.66),[33] thus leading to their incorporation within the solids as protonated ammonium ions. Besides, protonated SDAs will provide charge balance for the inclusion of low-valent Zn dopants in the networks. Therefore, protonated BP and BPM ammonium ions have been employed in our simulations of both the aqueous solutions and within the nanoporous solids. The atomic charges for BP and BPM cations (each with a net molecular charge of +1) were calculated by the charge-equilibration method.[34] In the aqueous solutions, the positive charge of the SDA molecules was compensated by including an equal number of Cl^- anions in the simulations. In the nanoporous solids, due to the lack of evidence from experiments about the location and distribution of dopants and/or other negatively charged structural defects, the SDA charge of +1 was compensated by uniformly reducing the charge of all the Al ions until charge neutrality. This model has been successfully applied to study related systems, mimicking in a realistic way the framework charges corresponding to a disordered incorporation of Zn in the lattice.[26,35] Only the Al charges were modified since Zn^{2+} ions are known to invariably replace Al^{3+} and not P^{5+} ions in the $AlPO_4$ lattices. Thereby, the atomic charges for P and O ions were fixed to 3.4 and −1.2, respectively, while charge for Al was gradually reduced from 1.4 until charge neutrality. The atomic charges in the water molecules were −0.82 and +0.41 for oxygen and hydrogen, respectively, which have been shown to describe well the properties of water containing systems.[36]

The aggregation behavior of the SDA molecules in water solution was studied by means of Molecular Dynamics (MD) simulations, under Periodic Boundary Conditions (PBC), using the Discovery code as implemented in Material Studio.[37] Two different concentrations [1 SDA:40 H_2O (1M) and 1 SDA:20 H_2O (2M)], corresponding to the experimental concentrations at which the different nanoporous structures are obtained, have been studied for each molecule. Sixteen (protonated) SDA molecules and 16 Cl^- anions were included in the simulation cell together with 640 water molecules (for 1 M concentration) or 320 water molecules (for 2 M concentration). The systems were initially geometry optimized to remove accidental overlapping of the molecules. An initial equilibration period has been allowed, consisting of 100 ps of MD simulations in the NPT ensemble at 298 K, using a Nose thermostat and a Berendsen barostat. This initial stage simulates the experimental preparation of the synthesis gels, which takes place at

(28) Dauger-Osguthorpe, P.; Roberts, V. A.; Osguthorpe, D. J.; Wolff, J.; Genest, M.; Hagler, A. T. *Proteins: Struct., Funct., Genet.* **1988**, *4*, 21.
(29) Moloy, E. C.; Cygan, R. T.; Bonhomme, F.; Teter, D. M.; Navrotsky, A. *Chem. Mater.* **2004**, *16*, 2121.
(30) Williams, J. J.; Smith, C. W.; Evans, K. E.; Lethbridge, Z. A. D.; Walton, R. I. *Chem. Mater.* **2007**, *19*, 2423.
(31) Garcia, R.; Philp, E. F.; Slawin, A. M. Z.; Wright, P. A.; Cox, P. A. *J. Mater. Chem.* **2001**, *11*, 1421.
(32) Hill, J. R.; Minihan, A. R.; Wimmer, E.; Adams, C. J. *Phys. Chem. Chem. Phys.* **2000**, *2*, 4255.
(33) Teitel'baum, A. B.; Kudryavtseva, L. A.; Bel'skii, V. E.; Ivanov, B. E. *Russ. Chem. B.* **1980**, *29*, 1571.
(34) Rappe, A. K.; Goddard, W. A., III *J. Phys. Chem.* **1995**, *95*, 3358.
(35) Gómez-Hortigüela, L.; Corà, F.; Catlow, C. R. A.; Blasco, T.; Pérez-Pariente, J. *Stud. Surf. Sci. Catal.* **2005**, *158*, 327.
(36) Williams, J. J.; Smith, C. W.; Evans, K. E.; Lethbridge, Z. A. D.; Walton, R. I. *Chem. Mater.* **2007**, *19*, 2423.
(37) *Discover module, Material Studio*, version 4.3; Accelrys Inc.: San Diego, CA, 2008.

ambient temperature and constant pressure (open systems). The density of the systems along this initial MD simulation was averaged, and a frame in the last steps of the MD trajectory with a density close to the averaged value was selected as the starting configuration for the subsequent study. Crystallization of the nanoporous materials occurs instead in autoclaves, that is, at constant volume (closed systems) and at high temperatures (473 K); accordingly, simulation of the synthesis gels were performed in the NVT ensemble at a temperature of 423 K. One-thousand picoseconds of MD simulations were run for every system, keeping the temperature constant with a Nose thermostat. Of this simulation time, the first 500 ps were assumed as the equilibration period, and only the last 500 ps of the MD simulations were used for production of results.

The aggregation behavior of the SDA molecules was studied by analyzing the Radial Distribution Function (RDF) of different sets of atoms [$g_{\alpha\beta}(r)$]. In addition, the concentration profiles were calculated according to the following equation:

$$n_{\alpha(\beta)}(r) = 4\pi\rho\beta \int_0^r g_{\alpha\beta}(r) r^2 \mathrm{d}r$$

where $n_{\alpha(\beta)}(r)$ is the number of β species surrounding α at less than a given distance (r), ρ_β is the bulk number density of atom β and $g_{\alpha\beta}(r)$ is the $\alpha-\beta$ RDF.

The stabilization provided by the occlusion of the organic SDA (BP and BPM) and water molecules when directing the crystallization of the AFI and SAO structures has been discussed previously.[26,27] In these works, we proposed a new computational model to study structure direction in the synthesis of hydrophilic aluminophosphate frameworks. The nanopores of hydrophilic AlPO structures can in fact be occupied not only by the organic SDA molecules but also by water that is always present as solvent in hydrothermal syntheses; the contribution of water to the energy crystallization must therefore be taken into account. Under thermodynamic control, the relative amount of water and organic SDA molecules is estimated by calculating the energy of the system at different SDA/water ratios in the nanopores. Since in the true synthesis SDA and water molecules do not come from vacuo but from the synthesis gel, we have to account for their stability in the gel in the final energetic balance (for a detailed explanation of the computational methodology, the reader is referred to refs 26 and 27). Our computational protocol allows us to estimate the total internal energy of the system as a function of the ratio between SDA and water molecules inside the nanoporous framework. The net stabilization can then be plotted as a function of the SDA content, using the following equation:

$$\Delta E_{\text{stab-SDA}}(n\text{SDA}) = E_f - n\text{SDA}(E^{\text{vac}}_{\text{SDA}} + E^{\text{sol}}_{\text{SDA}}) - n_{H_2O}(E^{\text{vac}}_{H_2O} + E^{\text{sol}}_{H_2O}) \quad (1)$$

where E_f refers to the internal energy (per T site) of the framework containing the SDA and water molecules, n_{SDA} and n_{H_2O} are the number of SDA and water molecules per T site, respectively, $E^{\text{vac}}_{\text{SDA}}$ and $E^{\text{vac}}_{H_2O}$ are the calculated energies of the molecules in vacuo, and $E^{\text{sol}}_{\text{SDA}}$ and $E^{\text{sol}}_{H_2O}$ are the energies of the SDA (at a given concentration) and water in aqueous solution, which represent consistent estimations of the stability of the SDA and water molecules in the gel. Plotting the value of $\Delta E_{\text{stab-SDA}}$ as a function of the number of SDA molecules per T site (n_{SDA}) enables us to estimate the most stable loading ratio of SDA and water molecules within the nanoporous frameworks, in equilibrium with their aqueous solution.

We then estimated the relative intrinsic stability of the open-framework AFI and SAO structures, which was related to that of the most stable AlPO framework, berlinite, isostructural to the α-quartz polymorph of SiO_2. The SAO, AFI, and berlinite framework energies were calculated via geometry optimizations by using the GULP[38] code and the potential from Gale and Henson.[39] The SAO and AFI framework energies were normalized per T site and related to that of berlinite (E_{framew}).

Our experimental results showed that the presence of Zn is necessary for the SAO structure to crystallize. This observation prompted us to estimate computationally which effect the incorporation of Zn has on the relative stability of AFI and SAO frameworks. This goal has been achieved by calculating the relative energy associated with a Zn^{2+}/Al^{3+} replacement in the AFI and SAO structures. We complemented the potential from Gale and Henson with new parameters for Zn−O interactions that we fitted to reproduce the framework structure of Zn-doped CHA (ZAPO-34) and AFI (ZAPO-5) materials obtained by quantum mechanical (QM) density functional theory (DFT) calculations. The latter have been performed with the hybrid-exchange B3LYP functional and the CRYSTAL code, using 1 Zn dopant per unit cell, charge-balanced by a Brønsted acid proton bonded to one of the four oxygens nearest neighbors to the Zn dopant. The newly fitted Zn−O potentials are able to reproduce Zn−O bond distances and the relative energy of the protonation sites in the CHA and AFI structures. Then, the energies of the Zn-doped AFI (1 Zn in a $1 \times 1 \times 2$ u. c., E_{ZnAFI}) and SAO (1 Zn in $1 \times 1 \times 1$ u. c., E_{ZnSAO}) structures were calculated by geometry optimization using the GULP code and these new parameters. While only one different crystallographic T site is available for AFI, SAO has 4 distinct positions where Zn can be located; all of them were studied, and the most stable one was taken. The computational methodology applied did not allow us to obtain absolute values for the replacement energies of Zn in the two structures; however, we can estimate the difference in the replacement energy between AFI and SAO using the following equation:

$$\Delta E_{\text{Zn/Al}}(\text{per Zn}) = (E_{\text{ZnSAO}} - E_{\text{SAO}}) - (E_{\text{ZnAFI}} - E_{\text{AFI}}) \quad (2)$$

where E_{SAO} and E_{AFI} refer to the framework energies of the undoped structures. Equation 2 yields the relative energy of doping the SAO compared to the AFI framework, expressed per Zn dopant.

Using all the relative energy contributions detailed above, the final crystallization energy relating the stability of AFI and SAO frameworks as a function of the SDA content has been computed as the energy of the open-framework structures relative to berlinite (E_{framew}) plus the stabilization energy provided by the occlusion of the SDA and water molecules ($\Delta E_{\text{stab-SDA}}$) plus the relative replacement energy of Al by Zn in the structures ($\Delta E_{\text{Zn/Al}}$). All the terms are expressed per T framework site, yielding:

$$\Delta E_{\text{cryst}}(n_{\text{SDA per T}}) = \Delta E_{\text{stab-SDA}}(n_{\text{SDA per T}}) + E_{\text{framew}} + n_{\text{Zn per T}}\Delta E_{\text{Zn/Al}} \quad (3)$$

The Zn content (n_{ZnperT}) in the SAO structure was assumed to be the same as the SDA content, as required for charge-balance purposes. The zero energy for eq 3 is that of undoped berlinite, as E_{framew} term relates AFI and SAO to berlinite; negative values of ΔE_{cryst} indicate that the nanoporous frameworks, under synthesis conditions, are thermodynamically favored compared to berlinite.

Results

1. Solution Chemistry. A. Fluorescence Studies of the Aggregation Behavior of BP and BPM in Aqueous Solution. UV−visible fluorescence spectroscopy is a powerful technique to study the supramolecular aggregation behavior of aromatic molecules that self-assemble through $\pi-\pi$ interactions of their aromatic rings. The π electronic system of the phenyl ring gives a fluorescence band centered at around 280 nm when the

(38) Gale, J. D. *J. Chem. Soc., Faraday Trans.* **1997**, *93*, 629.
(39) Gale, J. D.; Henson, N. J. *J. Chem. Soc., Faraday Trans.* **1994**, *90*, 3175.

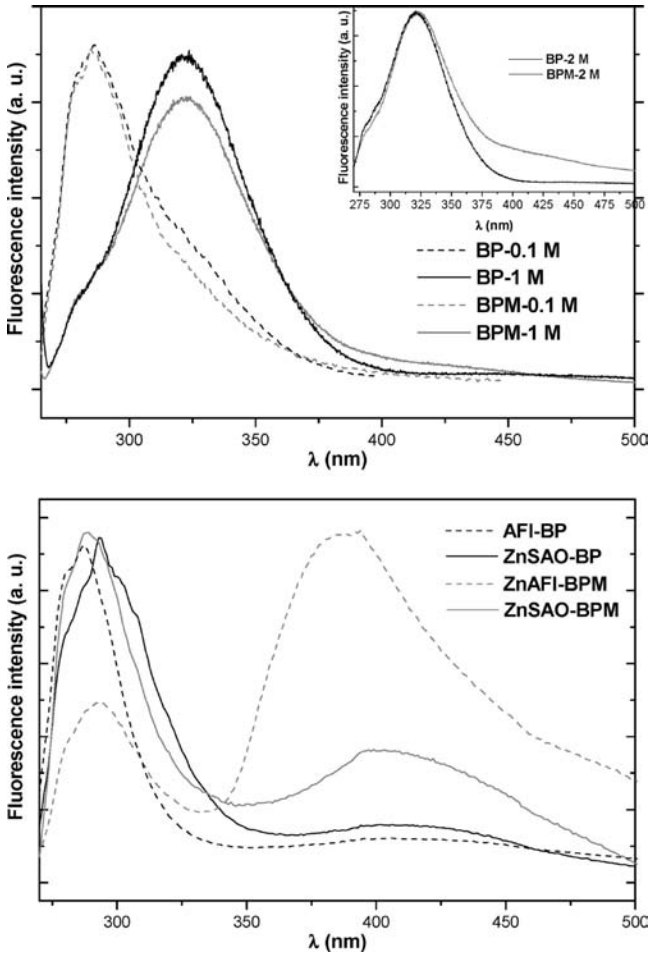

Figure 2. (Top) Height-normalized fluorescence emission spectra of BP chloride (black) and BPM chloride (gray) aqueous solutions at different concentrations (0.1 M in dashed lines and 1 M in solid lines). (Inset) Same spectra for a concentration of 2 M. (Bottom) Height-normalized fluorescence emission spectra of BP (black) and BPM (gray) in the AFI structure (dashed line) and in the SAO structure (solid line). The excitation wavelength was 260 nm.

molecules are arranged as monomers; this band is shifted to higher wavelengths when the molecules aggregate. Fluorescence spectra of the protonated BP and BPM chlorides at different concentrations are shown in Figure 2 (top). The spectra for BP (black) and BPM (gray) are very similar. At a concentration of 0.1 M, the main band observed is centered at 282 nm, which is assigned to the emission from BP and BPM monomers due to the low concentration at which this band predominates. However, a band at higher wavelengths (centered at 322 nm) can be appreciated, which becomes the predominant fluorescent band when the SDA concentration is increased to 1 M, although the band at 282 nm is still present as a small shoulder. The occurrence of this new band at 322 nm with the increase in the concentration of the molecules led us to assign it to the fluorescent emission from SDA molecules in an aggregated state. A further increase of the SDA concentration to 2 M does not vary further the fluorescence profile. In the spectra of BPM molecules, especially at the concentration of 2 M, a broad low-intensity band can be appreciated at around 400 nm; nevertheless, this band is also observed for BPM at very low concentrations (up to 10^{-4} M),[20] which suggests that this band is not due to higher-order aggregates. This low-intensity band appears intrinsically associated to the BPM molecule, but not to its aggregation state, although its assignment is not clear at the moment.

We can therefore conclude that the two SDA molecules in solution are mostly arranged in supramolecular aggregates of the same order (in terms of molecules composing the aggregate) at the concentrations at which the crystallization of the AFI (1 M) and SAO (2 M) nanoporous materials takes place. Surprisingly, no notable difference in the relative concentration of aggregated species has been found at the SDA concentrations of 1 and 2 M. However, it is interesting to note that, by comparing the fluorescence profile of the aggregate band (322 nm) of the two molecules, we can appreciate a slightly higher density of supramolecular aggregates for BP compared to BPM, especially at the lower concentrations of 0.1 and 1 M.

B. Computational Study of BP and BPM Aggregation in Aqueous Solution. Fluorescence spectroscopy can demonstrate the formation of aggregates, but it does not permit to study the particular intermolecular orientation in the aggregates that are formed. Therefore, we performed a computational study of the aqueous solutions at the temperature at which the crystallizations are carried out (423 K), to gain insights on the molecular features of the aggregates that the two molecules form in solution at the concentrations employed for AFI and SAO syntheses.

Depending on the relative orientation of the SDA molecules, four different types of intermolecular aggregates can form; these are depicted in Figure 3 (A to D). Two of them are arranged with parallel benzyl rings interacting through $\pi-\pi$ type interactions (A and B, which hereafter will be referred to as π-aggregates), differing in the relative orientation of the molecules that form the aggregate. In A, the pyrrolidine rings are located on opposite sides of the aggregate, while in B they are on the same side. In aggregate C, the aromatic ring of one molecule is interacting with the pyrrolidine ring of the other and, finally, in aggregate D, the two aromatic rings are coplanar in a side-ways interaction. Although the four types of aggregates listed above can form, the stabilization provided by the development of $\pi-\pi$ type interactions in the π-aggregates A and B makes them more likely to occur.

The molecular structure of the SDA molecules in monomeric or aggregated states in the solutions was analyzed via partial and total Radial distribution functions (RDF) calculated from MD trajectories. By analyzing the partial RDF of different sets of atoms around the SDA molecules, we can determine not only the aggregation state of the molecules but also the molecular structure of the SDA aggregates during the simulation. RDFs of different sets of atoms of BP (in black) and BPM (in gray) at concentrations of 1 SDA:20 H_2O (2 M, solid lines) and 1 SDA:40 H_2O (1 M, dashed lines) are plotted in Figure 4. The cp−cp RDF (Figure 4, top-left) describes the relative intermolecular distance between the C atoms of the aromatic rings (cp). We observe a clear peak with a maximum at ∼4.1 Å; this distance corresponds to the intermolecular separation in aggregates with benzyl rings parallel to each other, interacting through $\pi-\pi$ type interactions. The peak at ∼4.1 Å evidences a major formation of π-aggregates (A and B in Figure 3) for the two molecules. These π-aggregates are the ones that are observed by fluorescence spectroscopy, as discussed earlier; analysis of the structure of these dimeric aggregates reveals a deviation from a perfect sandwich dimer configuration (with coplanar aromatic rings and the transition dipole moments antiparallel to each other), condition which is required for efficient fluorescence of these aggregates. Results show that the

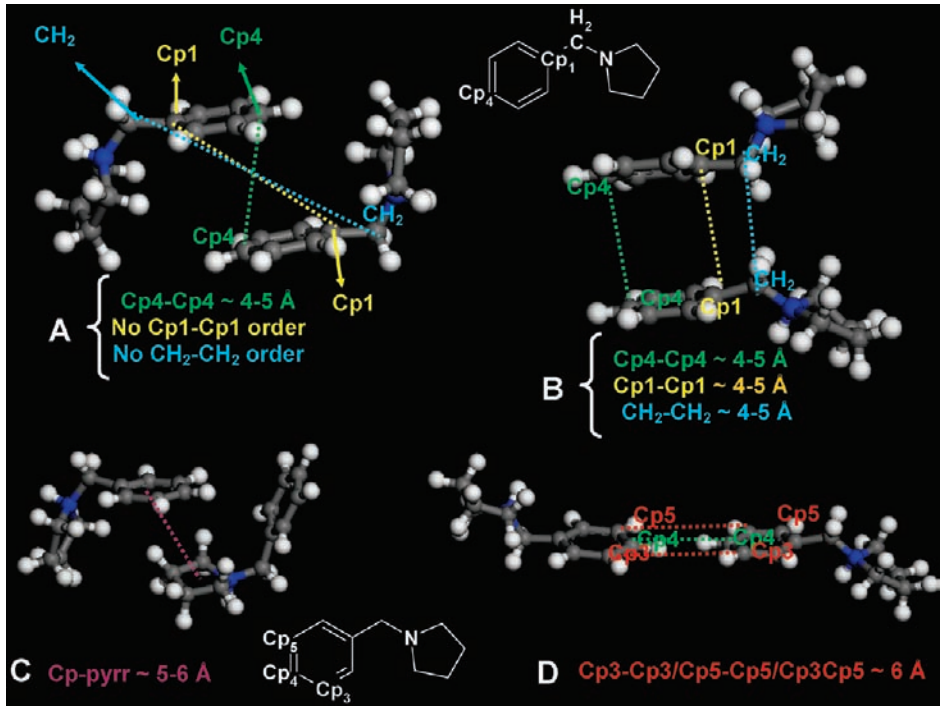

Figure 3. Illustration of the types of aggregates that the SDA molecules can form, showing the main distances that characterize them and that were analyzed with the RDF distributions to distinguish them in the simulations.

formation of these aggregates is higher for BP than for BPM molecules, in agreement with our experimental findings from fluorescence. It is interesting to note that no notable differences in the formation of aggregates are found as a function of the concentration. The concentration profile (Supplemental Figure 1, Supporting Information) shows that the coordination number, that is, the number of aromatic rings around a reference one, at a distance of up to ~6 Å (which corresponds to nearest neighbors in π-aggregates) is between 0.5 and 1, indicating that only dimers are present, and so higher order aggregates are not formed. However, the total cp−cp RDF distribution does not allow us to distinguish between the formation of A- and B-type aggregates.

To analyze in further detail the aggregate structure, we studied the RDF of individual aromatic C atoms, labeled as cp1 and cp4 in Figure 3. As shown in Figure 3, top, the intermolecular orientations of the molecules in A and B can be differentiated by analyzing the two partial RDFs of the aromatic C atoms in para position to the pyrrolidine group (cp4), of the ones bearing the substituents (cp1) and of the methylene C atoms (CH_2). In aggregate A, only a short-range order for the intermolecular cp4−cp4 distances around 4−5 Å is expected, while the much higher intermolecular distance between cp1−cp1, CH_2−CH_2 and cp1−CH_2 would cause the absence of short-range ordering in their respective partial RDFs. In contrast, the molecular orientation of the two SDA molecules in aggregate B would result in short (ordered) distances for each of the cp1−cp1, cp4−cp4, CH_2−CH_2 and cp1−CH_2 partial RDFs. Therefore, by analyzing the RDFs listed above, we can distinguish between the formation of A and B-type π-aggregates. Results for these RDFs are plotted in Figure 4. We observe that while the cp4−cp4 RDF is similar for BP and BPM molecules, with a peak for all the systems at around 4 Å, cp1−cp1 and cp1−CH_2 RDFs show important differences for BP and BPM molecules. In BP solutions, a clear peak can be observed for the cp1−cp1 distribution between 4 and 5 Å, and between 5 and 6 Å for the cp1−CH_2 distribution; in contrast, no short-range order peak is found for BPM neither in the cp1−cp1 nor in the cp1−CH_2 partial RDFs. Similar results are found for CH_2−CH_2 and N−N RDFs (Supplemental Figure 2, Supporting Information). These results evidence that BP molecules form both types of π-aggregates A and B, mostly B, while BPM form mostly A-type aggregates. Two snapshots of the MD trajectories, highlighting the presence of B-type π-aggregates in BP solutions and A-type π-aggregates in BPM solutions (at 1 M concentration) are shown in Figure 5.

Let us now consider the formation of C and D aggregates, without $\pi-\pi$ intermolecular interaction. We observe that the cp-pyrr RDF has a broad and low-intensity peak around 5−6 Å in BP solutions, while no indication of short-range order is found for BPM (Figure 4, bottom-left). A similar behavior is found for the RDFs considering the interaction between aromatic C atoms (cp) and N atoms (Supplemental Figure 2, Supporting Information), where a short-range order peak is observed for BP but not for BPM. These results suggest the presence, although at low concentration, of C-type aggregates in BP solutions, but not in BPM solutions. Finally, by analyzing the cp3cp5−cp3cp5 partial RDF (Figure 4, bottom-right), we observe a peak at ~4 Å originating from A and B-type π-aggregates, but no indication of short-range order at ~6 Å, which would occur in presence of D-type aggregates. The later result evidence the absence of D-type aggregates for both molecules, as expected.

To shed light on the different behavior observed for the two molecules, we examined in greater detail the interaction of the pyrrolidine ring, which is the molecular fragment that differentiates their molecular structure, with the solvent molecules. There are two polar groups in the SDA molecules that are responsible for a hydrophilic character and are expected to be more tightly solvated: the NH group of the pyrrolidine ring, present both in BP and BPM, and the OH group of the methanol subsituent, present only in BPM. Both can in principle form H-bonds with

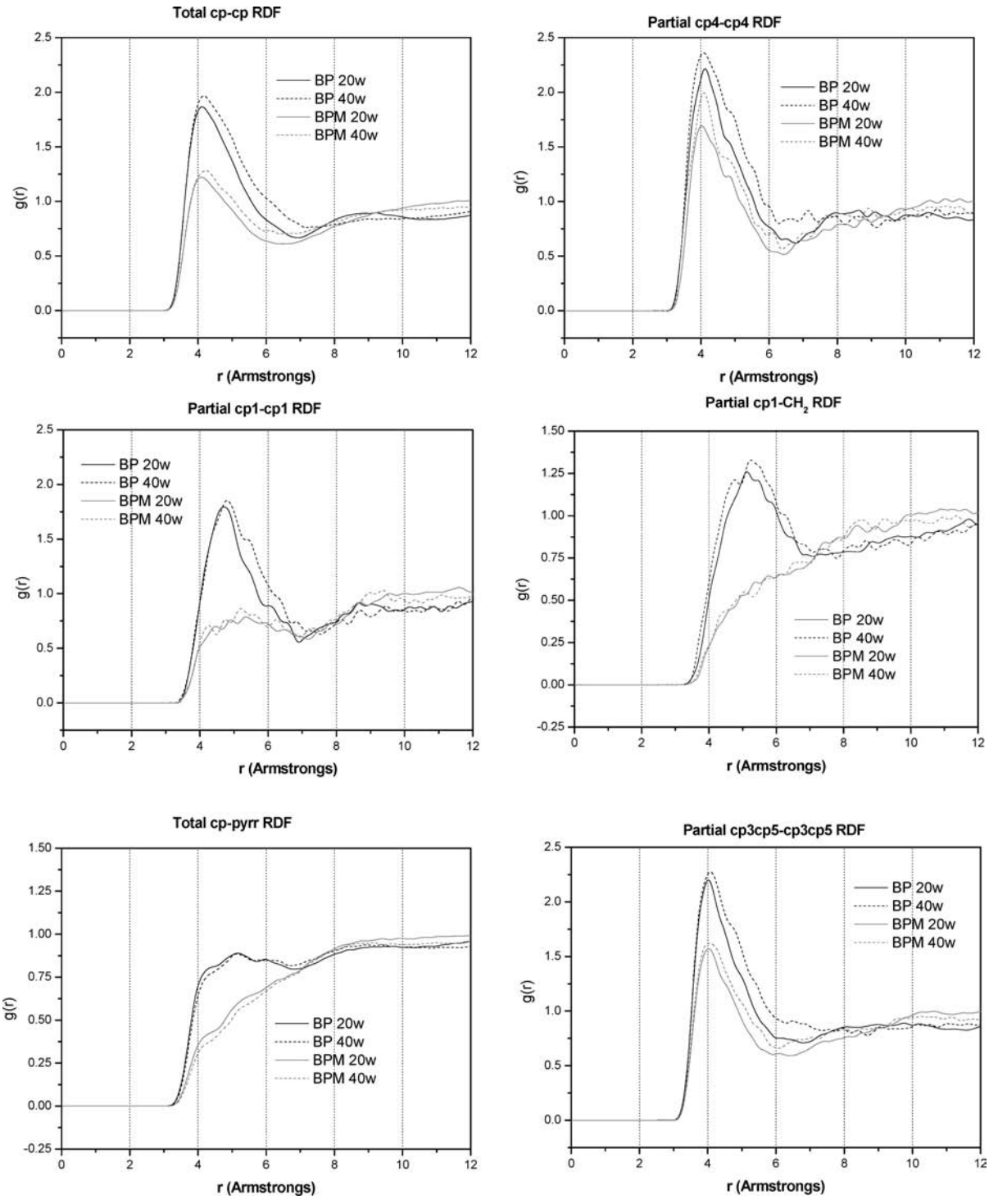

Figure 4. RDFs of different sets of atoms. (Top-left) Total intermolecular cp−cp RDF; (top-right) intermolecular cp4−cp4 RDF; (middle-left) intermolecular cp1−cp1 RDF; (middle-right) intermolecular cp1−CH_2 RDF; (bottom-left) intermolecular RDF between aromatic C atoms (cp) and pyrrolidine (pyrr) C (and N) atoms; (bottom-right) intermolecular RDF between cp3 and cp5.

water molecules. To characterize the solvation state of the ammonium (NH) and alcohol (OH) groups, we have calculated the RDFs between the N and O atoms of the SDAs and the water oxygens. These results are shown in Figure 6. We see that the water molecules surrounding the N atoms of the pyrrolidine rings have only a limited degree of short-range order: in both molecules, the peak at ∼3 Å, corresponding to H-bonded NH···O adducts, has a very low intensity. Water is instead very well-structured around the methanol group in BPM, showing a sharp and intense peak at 2.75 Å, corresponding to the formation of H-bonds with the alcohol groups of BPM. These results demonstrate that water has a much stronger interaction with the alcohol group of BPM than with the pyrrolidine ammonium group, possibly due to the conformational freedom and the low steric hindrance of the OH group in addition to the higher O electronegativity, in contrast to the N atoms that are in the central part of the SDA molecules and are part of a ring, which shields them from an effective interaction with the solvent. The stronger

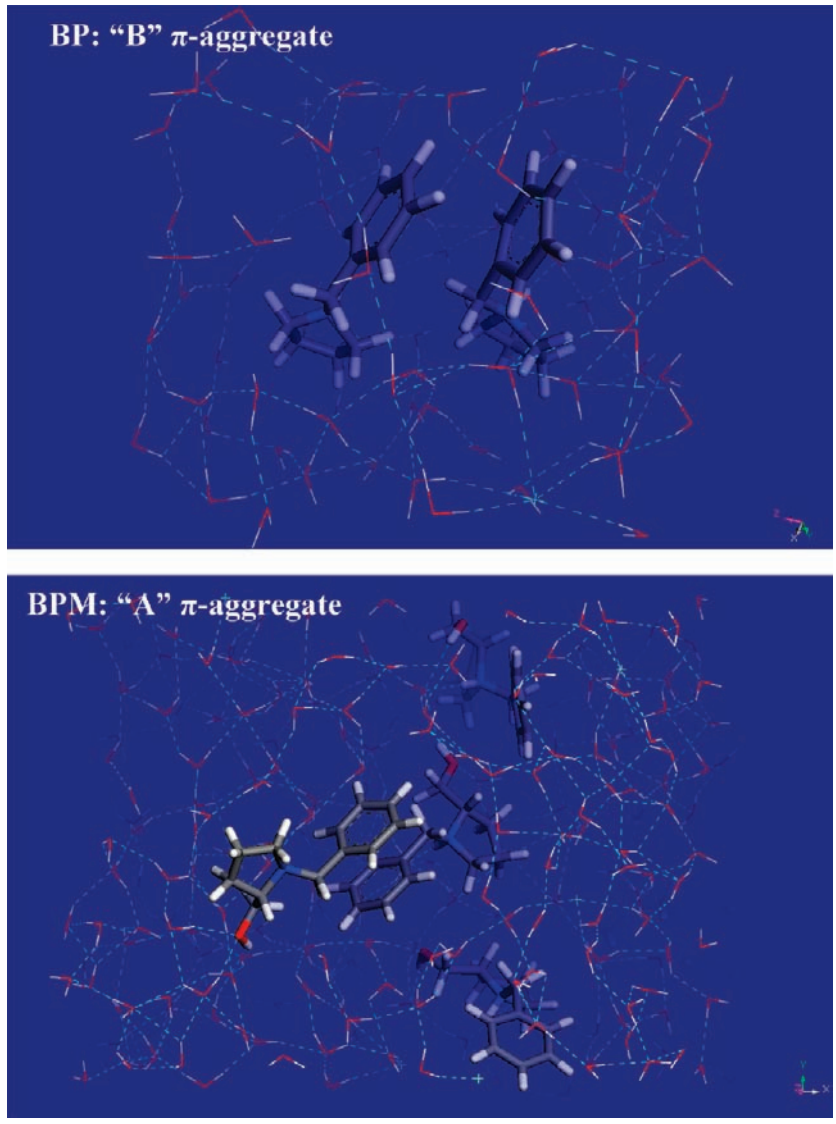

Figure 5. Snapshots of the MD trajectory showing the B (top) and A (bottom) π-aggregates of BP and BPM molecules, respectively.

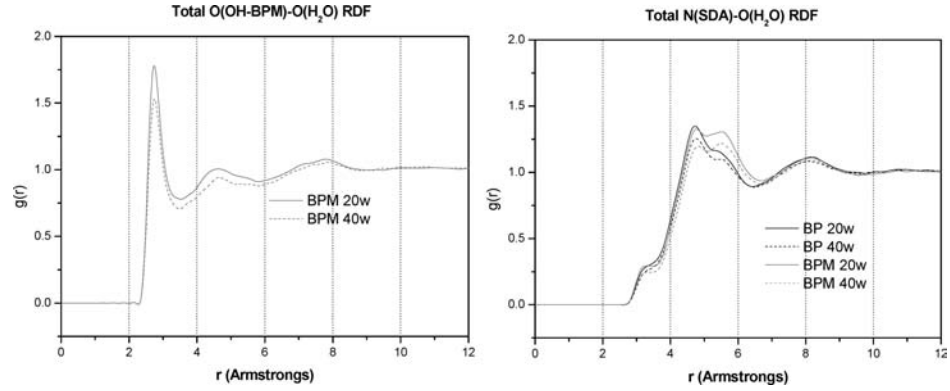

Figure 6. RDF between polar groups of SDAs and water molecules. (Left) RDF between O atoms of the methanol group in BPM molecules and O atoms in water molecules; (right) RDF between N atoms of the pyrrolidine ring in BP and BPM and O atoms in water molecules.

interaction with water of the methanol-functionalized pyrrolidine ring in BPM may explain the absence of B-type aggregates for this molecule: in BP solutions, the pyrrolidine rings are more hydrophobic and thus interact less strongly with water, which in turn results in a more favorable interaction between the hydrophobic pyrrolidine rings of different molecules, giving place to the appearance of B-type aggregates. A similar argument can explain the formation, although to a lower extent, of C-type aggregates. The pyrrolidine rings of the BPM molecules instead are hydrophilic and interact more strongly with water, thus making less favorable a pyrrolidine-pyrrolidine interaction and so limiting the formation of B-type (and of

C-type) aggregates; in fact, no interaction between the OH groups of different BPM molecules is observed (no short-range order peak in the OH−OH partial RDF distribution).

2. Synthesis and Molecular Occlusion in the AlPO Frameworks. A. Synthesis of AFI and SAO Frameworks. XRD patterns of the as-prepared samples revealed that pure-phase Zn-doped SAO frameworks crystallized at a SDA concentration of 2 SDA: 40 H_2O (~2 M) (hereafter called SAO-BP and SAO-BPM). The inclusion of Zn in the materials was found to be required to drive the crystallization toward the SAO structure; in the absence of Zn, an unknown structure that seems to be composed of a laminar framework is obtained. A lower SDA concentration (1 SDA:40 H_2O) led instead to the crystallization of the AFI structure.[23,24] Pure ZnAPO-5 was obtained with BPM as the SDA (AFI-BPM); however, a mixture of ZnAPO-5 and ZnAPO-36 was obtained after crystallization from Zn-containing gels with BP as the SDA. Therefore, a pure AlPO-5 material was also obtained from gels with the same BP concentration but in the absence of Zn for the sake of comparison, which will represent the AFI-BP system studied hereafter. Although required for the formation of the SAO structure, the presence of Zn is not the factor that controls the outcome of the synthesis as SAO or AFI; Zn-doped AFI frameworks are readily obtained experimentally at the correct SDA concentration for the AFI framework also in the presence of Zn. Therefore, we can confirm that the factor controlling the selectivity in the synthesis toward one of the two frameworks is the SDA concentration, which is the only factor differentiating the two gel compositions. The resistance of BP and BPM molecules to the hydrothermal treatments was assessed by CHN Elemental Analysis and ^{13}C CP MAS NMR. The incorporation of Zn in the frameworks was confirmed by ^{31}P MAS NMR.

The SDA contents for each host−guest system were determined from TGA and Elemental CHN Analysis, and were found to be 1.0 BP and 1.3 BPM molecules per unit cell in AFI[26] and 4.9 BP and 6.0 BPM molecules per unit cell in SAO.[25] A large water desorption is also observed by TGA, with a quantitative analysis revealing the presence of 5.6, 3.8, 22.3, and 13.6 water molecules per unit cell for the AFI-BP, AFI-BPM, SAO-BP, and SAO-BPM systems, respectively (note that the AFI ($Al_{12}P_{12}O_{48}$) and SAO ($Al_{28}P_{28}O_{112}$) unit cell sizes are different).

A kinetic study of the crystallization of the AFI structure revealed a faster formation of this framework when BPM is used as the SDA (crystallinity was 75 and 100% after 1 and 3 h heating, respectively) than when BP is employed (crystallinity was 60 and 93% after 1 and 3 h heating, respectively).[20]

B. Fluorescence Study of the Aggregation Behavior of BPM and BP Occluded in AFI and SAO. After characterizing the aggregation state of the BP and BPM molecules in solution, we proceeded to study their aggregation state inside the nanoporous frameworks. Solid state fluorescence spectroscopy results are presented in Figure 2, bottom. In these spectra, two distinct fluorescence bands can be observed, one centered at around 290 nm that corresponds to the presence of the SDA molecules as monomers, and one in the 350−450 nm wavelenght range which we previously demonstrated to be due to the presence of SDA dimers (formed in the ground state) occluded inside the framework pores.[20,21] The AFI structure obtained with BPM is the only case where SDA dimers are the predominant species; in the AFI structure obtained with BP, only a minor amount of dimers is present, while the majority of the SDAs are arranged as monomers. This difference is not due to the presence of Zn in the former case, since a similar situation is also observed for the undoped AFI structure obtained with BPM.[20] In contrast, a low dimer concentration of the SDA species occluded in the SAO structure is observed for both molecules. Nevertheless, the dimer concentration in this structure is higher for BPM than for BP, in concordance with the results observed in the AFI structure.

C. Computational Study of BPM and BP Occlusion within AFI and SAO. In this section we perform an energetic study of the stability of the two structures loaded with BPM and BP to understand the energetic parameters that govern the crystallization of the two framework types as a function of the SDA concentration.

Let us examine the individual energetic contributions to eq 3.

1. Framework Stability. The framework energies (relative to AlPO-berlinite) for the two open-framework structures were +1.01 and +3.04 kcal/mol per T site for AFI and SAO, respectively. The positive value of these energies demonstrates that these open-framework structures are intrinsically less stable than denser frameworks like berlinite, a feature that has long been recognized. Moreover, the results show that the low stability associated with open frameworks is much more pronounced in the SAO structure than in the AFI structure, consistent with its lower density. This observation evidences the intrinsic difficulty to direct crystallization during synthesis toward the SAO structure, and thus the necessity of very efficient SDAs to make the building-up of this open-framework viable. This is further experimentally evidenced by the infrequent crystallization of the SAO structure compared to the almost ubiquitous observation of AFI-type materials.

2. Stabilization Provided by Zn Doping. We studied the effect of the incorporation of Zn ions in both structures. Due to the difficulty in formulating a realistic chemical reaction model for the incorporation of Zn from the synthesis gel into the doped AlPO frameworks, we do not calculate absolute Zn/Al replacement energies, but only a relative value relating the ease of doping with Zn of the SAO structure compared to the AFI one, which is given by eq 2. The relative replacement energy ($\Delta E_{Zn/Al}$) was observed to be −3.2 kcal/mol per Zn ion in favor of the SAO structure. The latter finding indicates that Zn is better accommodated in the SAO framework, possibly due to its lower framework density that poses less pronounced constraints to atomic relaxation necessary to accommodate the large Zn dopants.

3. Host−Guest Interaction. The stabilization energies provided by the occlusion of the SDA and water molecules within the nanoporous frameworks have been discussed in detail in our previous publications.[26,27] We observe that in both structures the configuration with lowest energy contains a larger number of BPM than BP molecules. There is one arrangement of the BPM molecules in the AFI structure which is clearly more stable, which involves the formation of dimers located along the 12 MR channels (Figure 7, top), giving a packing value of 1.33 molecules per unit cell (0.055 SDA per T site); this agrees with and explains the high concentration of dimers observed by fluorescence. Instead, two different stable arrangements for BP molecules in AFI are found, one of them under a packing value of 1.33 molecules per unit cell, forming dimers in the same way as BPM; however, in this case a second stable arrangement is observed at a packing value of 1 molecule per unit cell (0.042 SDA per T site) (accompanied by the occlusion of 5.3 water molecules per unit cell in the 12 MR channel), in which the BP molecules are arranged as monomers (Figure 7,

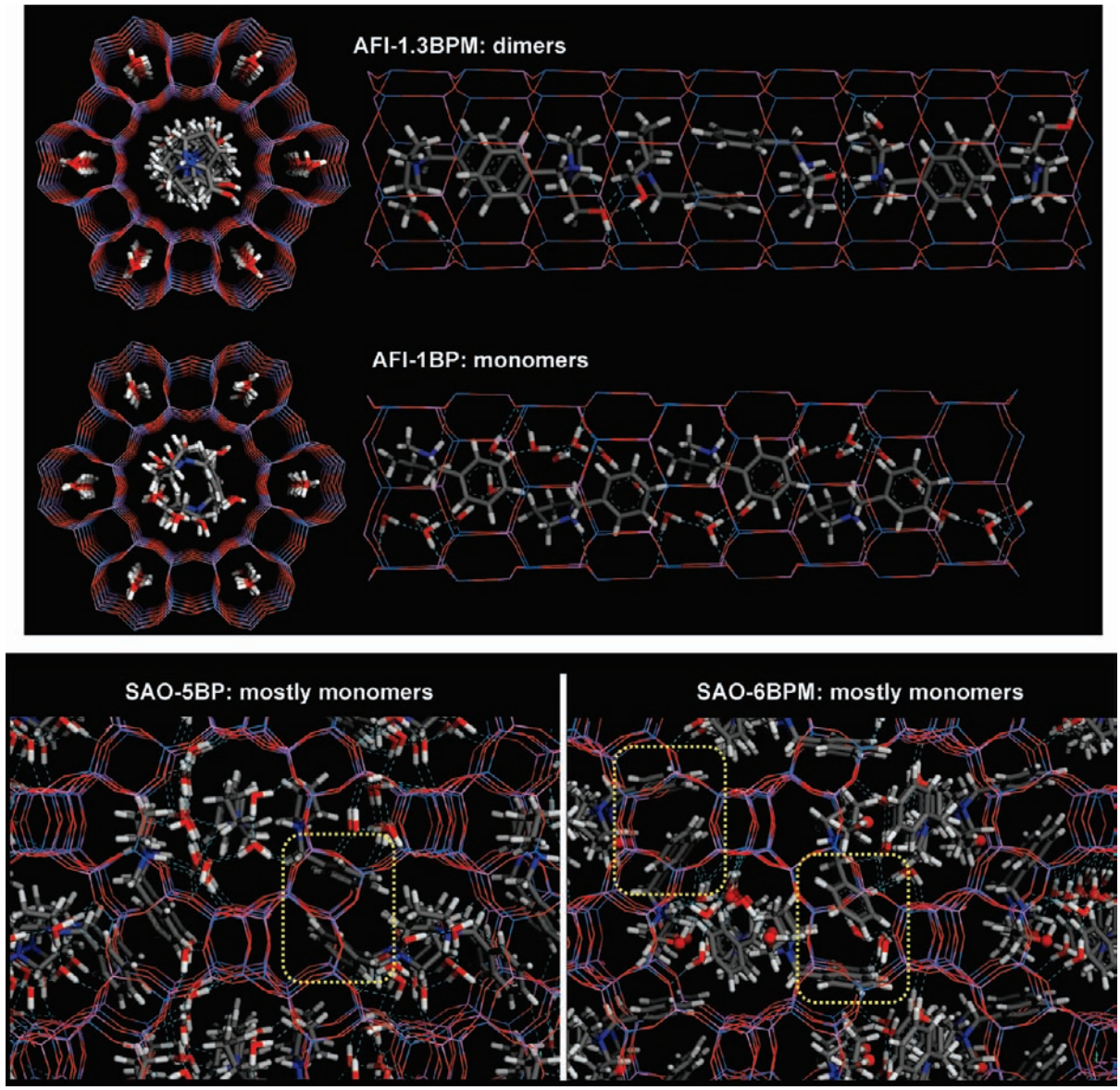

Figure 7. Most stable arrangement of the SDA molecules obtained by the computational study in the two nanoporous structures.

middle), with water molecules located as H-bonded chain clusters surrounding the SDA molecules. The crystallization energies of these two arrangements are very similar, and so both would be expected to occur under thermodynamic control; this result could at least partially explain the lower dimer concentration observed by fluorescence for this system. In the SAO structure, despite up to 8 molecules per unit cell can be accommodated, the more stable arrangement for BPM corresponds to the incorporation of 6 SDA and 9 water molecules per unit cell (0.107 SDA per T site), while a slightly lower SDA content is found in the most stable arrangement for BP, with 5 SDA and 22 water molecules per SAO unit cell (0.089 SDA per T site). The formation of dimers in the SAO structure is much less pronounced, as shown in Figure 7, bottom, due to the steric hindrance developed between molecules in the two perpendicular channel systems. Nevertheless, we can still appreciate the formation of dimers to a certain extent, which seems to be slightly higher in the BPM case (highlighted in dashed yellow rectangles in the figure), due to its higher SDA concentration. These results are once more in good agreement with the lower aggregation observed by fluorescence in this structure. The SDA and water contents predicted by our computational model are in very good agreement with the experimental values found by elemental CHN analysis and TGA, demonstrating the efficiency of our model in studying structure direction.

4. Total Crystallization Energy. The total crystallization energy (ΔE_{cryst}), including all the terms described above, was calculated as a function of the organic content per T site, following eq 3. The energy results for the two structures with each molecule are shown in Figure 8, while the most stable locations of the molecules were depicted in Figure 7. Table 1 summarizes several energetic and structural features of the most stable SDA contents for each host−guest system.

Despite the instability of the SAO and to a lesser extent of the AFI frameworks, the total crystallization energies for the two frameworks filled with the guest species are negative (between −1.4 and −1.9 kcal/mol per T site), indicating that all these host−guest systems are more stable than berlinite under our synthesis conditions. The low intrinsic stability of the

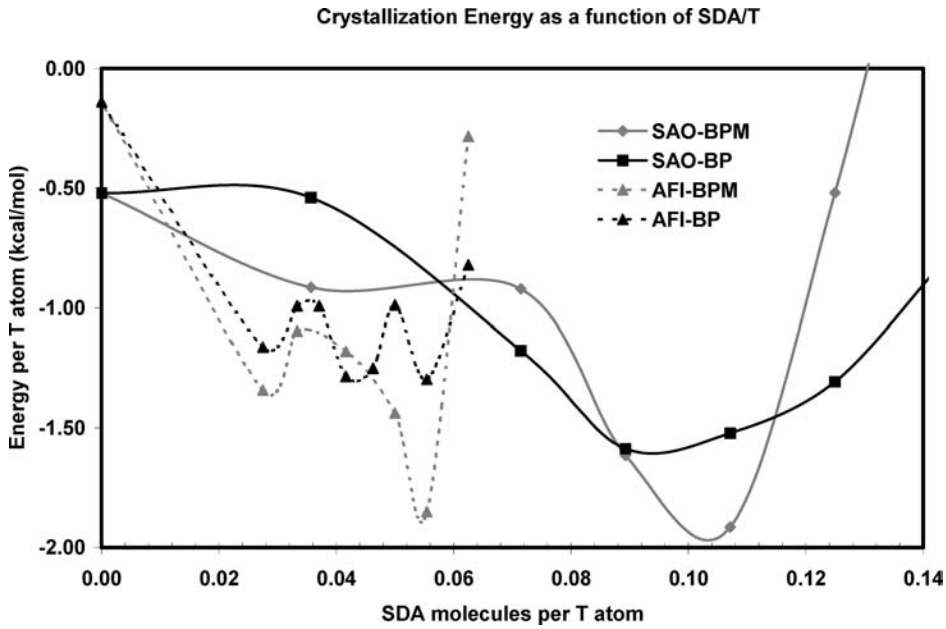

Figure 8. Total crystallization energy (in kcal/mol per T site, calculated from eq 3) as a function of the SDA per T site content, for the different host−guest systems.

Table 1. Comparison of Different Parameters in the SAO and AFI Structures Loaded with BPM or BP Molecules

property/system	SAO-BPM	SAO-BP	AFI-BPM	AFI-BP
Guest species (SDA and water molecules) content: experimental results				
SDA/u.c. (experimental)	6.0	4.9	1.3	1.0
H_2O/u.c. (experimental)	13.6	22.3	3.8	5.6
Guest species (SDA and water molecules) content: computational results				
SDA/u.c. (computational)	6	5	1.33	1
H_2O/u.c. (computational)	9	22	4	9.3
T sites/u.c.[a]	56	56	24	24
SDA/T	0.11	0.09	0.06	0.04
SDA/T (gel)[b]	0.50	0.50	0.25	0.25
H_2O/T	0.16	0.39	0.17	0.39
H_2O/SDA	1.5	4.4	3.0	9.3
Free volume occupied by guest species				
Zeolite free V/T[c]	43.7	43.7	29.9	29.9
Occupied V fraction[d]	0.56	0.52	0.47	0.48
SDA density (per 1000 Å^3) (framework)	1.49	1.25	0.96	0.72
SDA density (per 1000 Å^3) (gel)[e]	1.12	1.15	0.68	0.69
SDA density ratio (framework/gel)	1.33	1.09	1.41	1.04
Relative contributions to the total crystallization energy				
Stabilization (SDA) E/T (eq 1)[f]	−4.60	−4.33	−2.86	−2.30
Framework E/T	+3.03	+3.03	+1.00	+1.00
Relative replacement E/T (eq 2)	−0.34	−0.29	0	0
Crystallization E/T (eq 3)	−1.57	−1.40	−1.93	−1.37

[a] 'T' refers to tetrahedral framework atoms (P and Al); [b] SDA/T ratio in the synthesis gel. [c] Free volume in the nanoporous framework (in Å^3 per T site). [d] Fraction of volume occupied by the SDA+water molecules divided by the total free volume of the nanoporous framework. [e] Calculated from simulations of the solutions. [f] Stabilization energy is taken at the most favorable SDA/water ratio. All of the energies are given in kcal/mol per T site.

frameworks (ΔE_{framew}) is efficiently compensated by the host−guest interaction energy of both SDA and water molecules. The stabilization provided by the occlusion of the guest species in the SAO structure (−4.6 and −4.3 kcal/mol per T site for BPM and BP, respectively) is much higher than that in the AFI structure (−2.9 and −2.3 kcal/mol per T site for BPM and BP, respectively). This is due to the higher void volume available to occlude guest species in the SAO structure (43.7 Å^3 per T site) than in the AFI structure (29.9 Å^3 per T site). This results in much higher SDA contents in SAO (around 0.1 SDA per T sites) than in AFI (around 0.05 SDA per T site), condition that is required to overcome its high framework instability.

Interestingly, the ratio between the SDA contents in the two frameworks (around 2:1 in SAO:AFI) is the same as the ratio of the SDAs in the synthesis gels for the two structures. In contrast, the water contents are very similar for each molecule in the two structures: the frameworks obtained with BPM lead to a water content of around 0.16 H_2O molecules per T site, while a much higher water content is observed in both types of frameworks when BP is used as the SDA, around 0.4 H_2O per T site. It is also interesting to note that, for a given SDA molecule, a relationship exists between the H_2O/SDA ratio in the two structures and in the corresponding synthesis gels. For BPM, the H_2O/SDA ratio goes from 3 in AFI to 1.5 in SAO (changing by a factor of 2.0), while for BP it goes from 9.3 to 4.4 (changing by a factor of 2.1); these values are the same as the variation of the H_2O/SDA ratio in the gels for AFI and SAO (40:20, with a change by a factor of 2.0). The H_2O/SDA ratios cover therefore a different range in AFI and SAO, but parallel the modification in the synthesis gel, evidencing that the changes in the concentration of the gels are somehow reproduced in the crystals obtained.

D. Correlation between the SDA Density in the Gels and in the Frameworks. The concentration profiles of the SDA and water molecules in the different solutions follow a similar pattern than the ones of the SDA molecules and framework oxygen atoms in the nanoporous structures they direct (Figure 9): BP and BPM concentration profiles in 1 M solutions are related to those in the AFI structure; the same correspondence is found for 2 M solutions and the SAO structure. Moreover, the SDA densities (per volume) in the frameworks and in their corresponding solutions (gels) also follow a similar trend (Table 1), evidencing a relationship between the SDA concentration (density) in the gel and in the framework. This match reinforces the concept that the SDA molecules in the gels determine an exclusion zone (where the AlPO species cannot be located) around which the pores and/or cavities of the nanoporous framework arise during crystallization. The zone occupied by water molecules will instead represent the space where the AlPO species will locate and condense to form the nanoporous

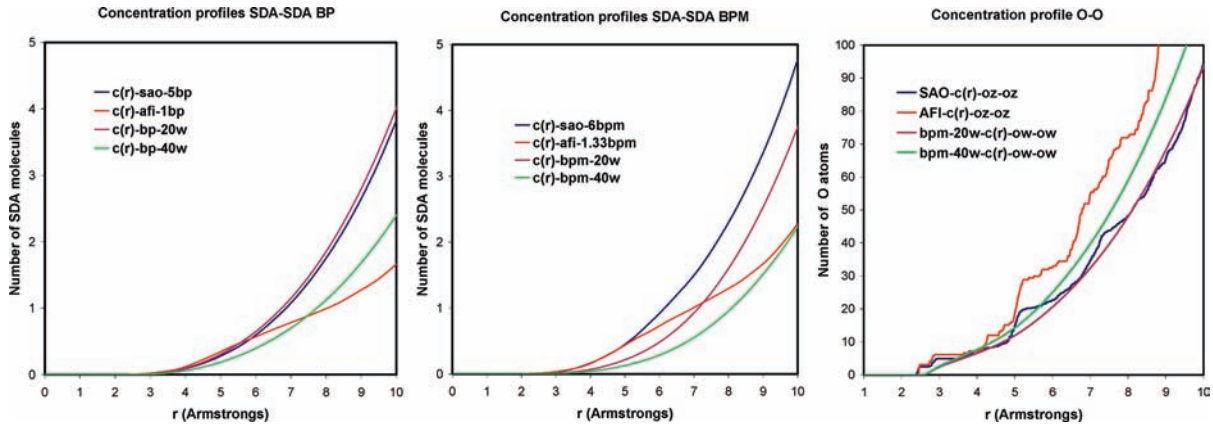

Figure 9. Concentration profiles of SDA−SDA molecules (left, BP; middle, BPM) and of O−O distances (right, O(water)−O(water) distances in solution and O(framework)−O(framework) in zeotypes).

framework around the SDAs; indeed, the density of water molecules surrounding those exclusion zones is very similar to the framework O density in the zeotype materials (Figure 9, right). These observations suggest that the density of the nanoporous material (and so its porous network) is controlled by the arrangement and the density of the SDAs in the gels, i.e., by the SDA/water ratio. Nevertheless, it is important to note that the SDA density is slightly higher in the framework than in the synthesis gel for BPM, while it is similar in both media for BP. This means that during crystallization the BPM molecules tend to pack more densely to maximize the occlusion of SDA species in the framework, a feature driven by their high interaction with the frameworks.

The structural relationship between the arrangement of the SDA molecules and O atoms in solution (water O atoms) and in the framework (framework O atoms) is supported by the analysis of the RDF distribution of aromatic C atoms (cp) and oxygen atoms in solution (water) or in the structures (framework O) (Supplemental Figure 3, Supporting Information). We observe that the location of the first shell of water molecules surrounding the aromatic rings in solution (at around 3.5 Å) is similar to that of framework O atoms in the AFI structure (see Figure 11).

It is also important to note, in Figure 8, that the crystallization energy favors the AFI over the SAO polymorph for ratios between SDA molecules and T atoms of the framework up to ~0.06 (i.e., approximately 1 M SDA concentration in solution), while SAO becomes energetically stable at higher SDA molar ratios. The molar/SDA concentration in the synthesis gel has therefore a primary effect in deciding which polymorph will form. The correspondence between SDA density in solution and framework may have a strong kinetic origin: a large local change of SDA concentration in the forming nuclei of the framework requires the creation of concentration gradients in the surrounding gel, which can be expected to be slow and opposed by entropic factors, especially if SDA molecules need to be expelled from the forming nuclei (if the SDA concentration is lower in the solid than in solution). The SDA molecules expelled from the nuclei will form a barrier that prevents access of new Al/P species to the nuclei, required for crystal growth. Setting a higher than required SDA density in the synthesis gel compared to the optimal SDA density in the targeted framework will require slow SDA diffusion processes in solution, and will yield the desired framework only if no alternative structure is available at the higher SDA density (such as the SAO structure in the case discussed here).

Discussion

On the basis of the results presented in the previous sections, we can relate the aggregation behavior of the SDA molecules in the aqueous solutions to their mode of incorporation within the nanoporous frameworks. Indirectly, this comparison may shed light on the important issue of whether the supramolecular aggregates are the true SDA in the AFI and SAO syntheses or the dimers form only inside the solid once the structure is obtained, using monomeric BP and BPM molecules in the structure-directing step. The former case is to be preferred, as control/design of the supramolecular aggregation would enable us to use simpler (and cheaper) molecules as SDA in the synthesis of large-pore nanoporous structures.

The fluorescence spectroscopy results of the SDA molecules incorporated inside the SAO and, especially, the AFI frameworks show a higher concentration of dimeric aggregates for the BPM molecules compared to BP. However, fluorescence results of the SDA solutions show the opposite trend: BP aggregates to a larger extent than BPM. There is therefore an apparent contradiction between extent of aggregation in solution and in the solids. Our multilevel approach provides however a more complete picture of the problem.

Both thermodynamic and kinetic factors can influence the structure direction mode of the organic SDA molecules, and thus their final occlusion within the crystallized nanoporous frameworks. First, our computational model for structure direction led us to gain insights into the thermodynamics of the occlusion of guest species (both SDA and water) in the nanoporous frameworks. Figure 8 shows that BPM has a strong preference to be incorporated in the AFI structure as dimers; fluorescence spectra confirm the high aggregation of BPM in the AFI structure. However, the BP-AFI loading curve presents two minima with similar stabilities at loadings of 0.055 and 0.042 SDA molecules per T site, corresponding to the inclusion of dimers (1.33 molecules per unit cell) and monomers (1 molecule per unit cell), respectively. These results provide a thermodynamic rationale for the higher aggregation observed for BPM than for BP in the AFI structure. The low BP aggregation in AFI experimentally observed is however surprising, taking into account that the incorporation of the molecules as dimers (0.055 per T) and monomers (0.042 per T) is equally

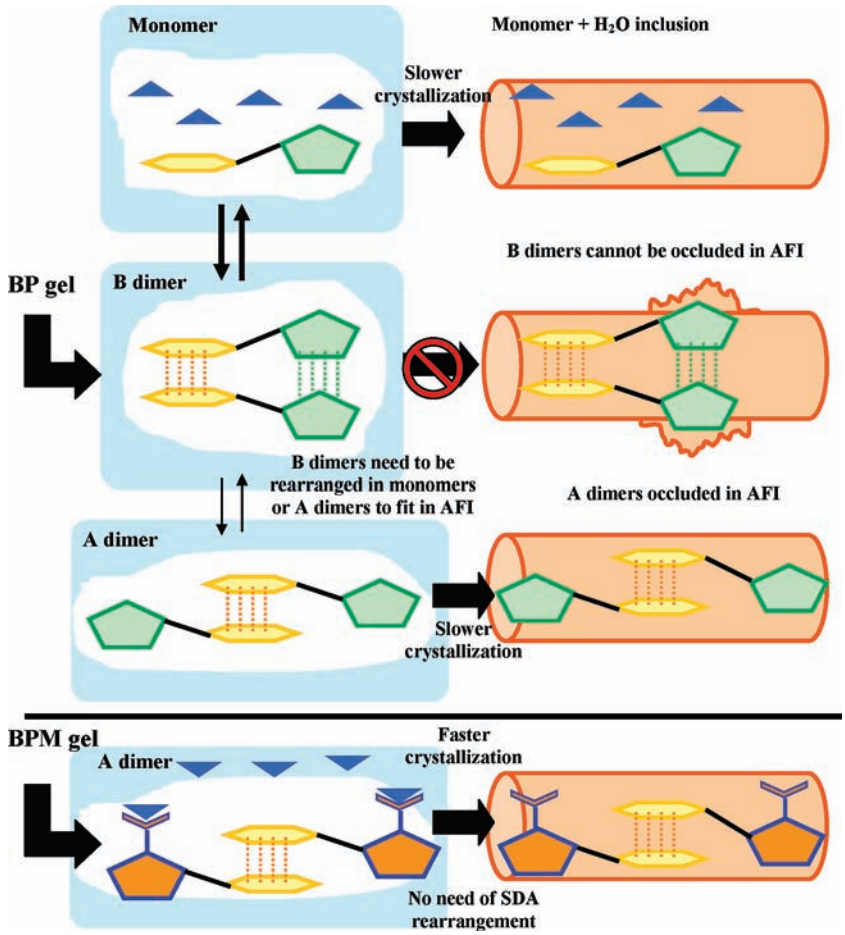

Figure 10. Illustration of the proposed mechanism of structure direction for BP (top) and BPM (bottom) of AFI. BP forms initially B-type dimers that cannot fit within the AFI dimensions, and so they need to rearrange into either monomers (mostly) or A-type dimers to fit in the AFI channels, leading to a slower crystallization rate. Instead, BPM forms A-type dimers that are directly incorporated in the AFI structure.

stable and that BP molecules show stronger aggregation in solution (Figure 2). An explanation for the low concentration of BP dimers in AFI is provided by kinetic effects, i.e., by the *type* of aggregates present in the solutions. BP molecules in solution form the two types of π-aggregates, mostly B, and also, although to a lower extent, C-type aggregates. However, considering the molecular structure, only A-type aggregates can be accommodated within the one-dimensional channels of the AFI structure. The B-type aggregates are too large to fit inside the AFI channels, since the space occupied by the two pyrrolidine rings on the same side of the dimer is larger than the diameter of the cylindrical AFI channels. For BP molecules to be occluded in the AFI channels, B and C dimers must therefore rearrange into A-type aggregates or more likely separate into monomers, a feature that would slow the crystallization of the structure, as observed in the kinetics of crystallization experiments, and would result in a major occlusion of BP monomers, as also experimentally observed. Instead, A-type aggregates are the predominant species in BPM solutions; they can be readily incorporated into AFI, and are the likely SDA in the gels. No rearrangement is required, thus explaining the high concentration of BPM dimers in the AFI channels and its faster crystallization. The reason for the different aggregation behavior of BP and BPM is found in the hydrophilic methanol group present in the pyrrolidine ring of BPM: the alcohol group is strongly solvated, thus leading to an ordering of water around the pyrrolidine ring; such strong pyrrolidine−water interaction prevents intermolecular pyrrolidine−pyrrolidine interactions (observed in B aggregates) and thus drives the aggregation of BPM molecules into A-type dimers. The N atoms of the pyrrolidine rings (both in BPM and BP) do not strongly interact with water since they are part of a ring and poorly available to interact with the solvent. The pyrrolidine rings of BP have hydrophobic nature, and thus tend to interact with pyrrolidine rings of other BP molecules, giving place to B-type aggregates, and even with benzyl rings, giving place to C aggregates, that need to rearrange for occlusion into AFI to occur. All these observations are schematically illustrated in Figure 10. These findings indicate the existence of kinetic barriers that limit and slow-down the incorporation of BP dimers into the AFI channels and rationalize the relative concentration of monomeric and dimeric BP and BPM species in AFI.

Fluorescence in solution shows that the aggregation state of the SDA molecules is identical at the two concentrations of 1 and 2 M employed for AFI and SAO syntheses. We observe that the AFI-BPM host−guest system is the one where the highest formation of dimers is found; in addition, we observe in both structures a stronger trend for BPM to form dimers. These results demonstrate that the occlusion of the SDAs as aggregated species does not depend only upon the formation of aggregates in the gels prior to crystallization. Instead, the molecular orientation of the aggregates formed, the topology of the channels and/or cavities of the nanoporous framework as well as the interaction of the molecules with the network all

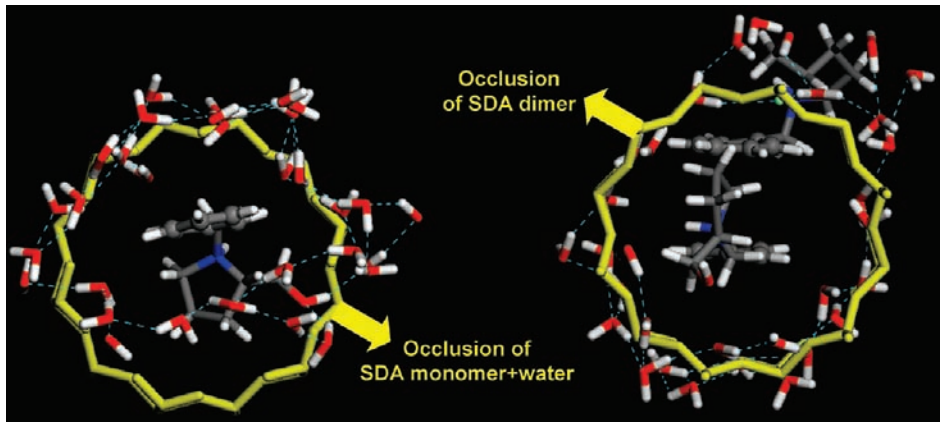

Figure 11. Snapshots of the MD trajectory of BPM molecules (1 M solution), showing the arrangement of water molecules (in the first next-nearest neighbor solvation shell) around the aromatic atoms (displayed as balls) of BPM monomers (left) and BPM dimers (right). The AFI channel atoms are also shown (displayed in yellow) overlapped to highlight the structural relationships.

influences the dimer occlusion, and so the mode of structure direction of the SDA molecules through single or supramolecular entities. The larger diameter of the AFI channels (7.3 × 7.3 Å in AFI vs 6.5 × 7.2 Å and 7.0 × 7.0 Å in SAO) and their one-dimensional nature explains the better accommodation of BPM dimers.

A higher occlusion of SDA molecules and a lower incorporation of water are found when BPM directs the crystallization of the nanoporous frameworks. Indeed, the H_2O-to-SDA ratio is much lower for BPM-directed AFI and SAO frameworks than for the corresponding BP-systems (Table 1). This behavior is explained by the more hydrophilic nature of BPM, which interacts more strongly with the hydrophilic AlPO frameworks, thus leading to a higher structure directing efficiency of BPM compared to BP. The BPM molecules perform therefore a dual action in structure direction, where they template and strongly stabilize the structure, which results in a major incorporation of BPM molecules in the nanoporous frameworks. BP molecules, instead, yield lower interaction energy, and require a cooperative action in which the organic molecules play a templating role to hold the nanoporous architecture, while the water molecules provide further strong stabilization to the host−guest systems.

The different mode of structure direction involving monomers or dimers is further illustrated by the arrangement of water molecules surrounding the aromatic rings in solution, which in Figure 11 is related to the arrangement of the framework atoms in the AFI 12 MR channels (yellow atoms). The solvation sphere around the dimer has a very similar structure to the AFI channel (Figure 11, right), suggesting a high efficiency of dimers in directing this framework. Indeed, dimers seem to be necessary for the AFI structure to nucleate, as proposed in our previous work,[20] possibly due to the close structural relationship between water-solvated dimers and AFI-occluded SDA dimers. This would suggest that, in the course of the crystallization, the AlPO species will gradually displace the water molecules surrounding the SDAs, leading to the host−guest species from which the nanoporous materials will arise, in agreement with the long-time proposed structure direction mechanisms.[40−44] When monomers are occluded, instead, several water molecules are simultaneously incorporated in the large AFI channels (Figure 11, left), as observed experimentally with BP, to completely fill the subsequent void space.

The intrinsically lower stability of open-framework structures requires some type of strong stabilization to make the crystallization viable; this is provided by the occlusion of both SDA and water molecules within the nanoporous frameworks, which strongly interact with the pore walls. The framework energy of the SAO structure (3.0 kcal/mol per T site) is much higher than that of the AFI structure (1.0 kcal/mol per T site), indicating that the former is much more difficult to be built up. In contrast, the stabilization provided by the occlusion of the organic and water molecules is much higher in the SAO (between −4 and −5 kcal/mol per T site) than in the AFI structure (between −2 and −3 kcal/mol per T site). This higher stabilization energy in the SAO structure is due to the higher free volume available in its structure, and consequently to a higher occlusion of guest molecules within the framework. Therefore, a balance between the lower intrinsic stability of the most-open frameworks and their higher void space available to host guest molecules is apparent, provided the void space is efficiently filled by strongly stabilizing guest species. The higher instability of SAO becomes evident from the experimental observation that this open framework structure is not stable upon calcination, i.e., upon removal of the guest species, evidencing the intrinsic instability of the structure and the necessity of the occlusion of guest molecules to hold the porous architecture. Instead, the AFI structure is stable upon calcination. Thus, the requirement of a larger stabilization for building the SAO framework results in the experimental requirement of increasing the SDA concentration to 2 SDA:40 H_2O to accomplish its crystallization. In fact, the relationship between the SDA density in solution and in the framework that we have observed, if proven of more general validity, may provide a synthetic control of the porosity of the produced materials by adjusting the SDA-to-water ratio in the gels.

Conclusions

A different aggregation behavior of BP and BPM molecules in the structure direction of the AFI and SAO structures has been found; BPM molecules show a higher occlusion as dimers, especially in the AFI structure. However, BPM molecules show a lower aggregation in solution. These apparently contradictory observations can be explained by a combination of thermody-

(40) Flanigen, E. M.; Bennett, J. M.; Grose, R. W.; Cohen, J. P.; Patton, R. L.; Kirchner, R. L.; Smith, J. V. *Nature* **1978**, *271*, 512.
(41) Chang, C. D.; Bell, A. T. *Catal. Lett.* **1991**, *8*, 305.
(42) Burkett, S. L.; Davis, M. E. *J. Phys. Chem.* **1994**, *98*, 4647.
(43) Burkett, S. L.; Davis, M. E. *Chem. Mater.* **1995**, *7*, 920.
(44) Burkett, S. L.; Davis, M. E. *Chem. Mater.* **1995**, *7*, 1453.

namic and kinetic effects: the higher loading of the BPM molecules within the nanoporous frameworks is related to their higher interaction with the oxide networks, owing to the presence of the strongly interacting hydrophilic methanol groups. Meanwhile, kinetic effects are related to the different molecular shape of the aggregates in solution: while BPM forms only one type of aggregate whose dimensions are suitable for being incorporated within the pores of the frameworks, and in particular in AFI, BP forms aggregates with different intermolecular orientations, of which only one can be accommodated in the frameworks, thus reducing the chance to incorporate aggregated species.

Our results demonstrate that it is impossible to establish a simple correlation between the aggregation behavior of the molecules in solution and the eventual incorporation of these aggregates in the frameworks. This is well illustrated by the fact that SAO incorporates less dimers than AFI, despite being synthesized with a higher SDA concentration. A number of factors, including the topology of the framework, the intermolecular orientation within the aggregates, the interaction with the network, as well as the aggregation behavior itself, governs the occlusion of dimers in nanoporous materials, and thus determine the mode of structure direction through single or supramolecular SDA entities.

We have observed that structure direction of BPM involves a major occlusion of SDA molecules (mostly dimers in the case of AFI), that play a dual role as templates and stabilizing agents, while structure direction of BP involves a combined occlusion of the SDA and water, leading to a cooperative structure directing action where BP templates the structure and provides a certain stabilization and water enhances the stabilization by developing strong interactions with the hydrophilic frameworks.

Our work confirms the important role that the organic SDA molecules play in the crystallization of open-framework materials. The high instability associated to low-density materials is compensated by the occlusion of guest species, both organic and water molecules in the case of $AlPO_4$-type materials. This is especially true in the SAO synthesis, whose large framework instability is well compensated by a very efficient filling of its large void volume by guest (SDA and water) molecules.

In addition, our study allows us to raise an interesting point for the synthesis of new large-pore structures: the SDA density of the nanoporous materials, and so the void space available in the porous network, can be controlled, at least to a certain extent, by the SDA density in the gels, which in turn is controlled by the SDA/H_2O molar composition of the synthesis gels.

As a main conclusion drawn by our multitechnique approach, we can say that the SDA$-H_2O$ arrangement dictated by the gel chemistry, which we simplify to be the SDA$-H_2O$ system, needs to be approximate to the physicochemical properties of the crystallizing material. In other words, what happens in the gel, relating to the SDA aggregation behavior and the connected kinetic effects and the water$-$SDA arrangement, must foresee what is going to happen in the final crystals. This implies that the concept of using self-aggregating aromatic SDAs is indeed a useful tool to get large-pore nanoporous materials since the behavior of these SDAs in the gel is directly related to that in the final crystal. Moreover, computational studies like the present could aid in rationally choosing the most suitable self-assembling molecules to optimize the aggregation.

Acknowledgment. L.G.H. and A.B.P. are grateful to the Spanish Ministry of Science and Innovation for postdoctoral and predoctoral grants, respectively. Financial support of the Spanish Ministry of Education and Science (project CTQ2006-06282) is acknowledged. FC is supported by an RCUK Fellowship. We also thank Accelrys for providing their software and Centro Técnico de Informática for running the calculations.

Supporting Information Available: Additional RDFs and concentration profiles. This material is available free of charge via the Internet at http://pubs.acs.org.

JA906105X